Available online at www.sciencedirect.com

ScienceDirect

journal homepage: www.elsevier.com/locate/he

Laser induced formation of copper species over TiO_2 nanotubes towards enhanced water splitting performance

Katarzyna Grochowska [a], *Zuzanna Molenda* [a], *Jakub Karczewski* [b], *Julien Bachmann* [d,e], *Kazimierz Darowicki* [c], *Jacek Ryl* [c], *Katarzyna Siuzdak* [a,*]

[a] *Centre for Plasma and Laser Engineering, The Szewalski Institute of Fluid-Flow Machinery, Polish Academy of Sciences, Fiszera 14 St., 80-231, Gdańsk, Poland*

[b] *Faculty of Applied Physics and Mathematics, Gdańsk University of Technology, Narutowicza 11/12 St., 80-233, Gdańsk, Poland*

[c] *Faculty of Chemistry, Gdańsk University of Technology, Narutowicza 11/12 St., 80-233, Gdańsk, Poland*

[d] *Faculty of Sciences, University of Erlangen-Nuremberg, Cauerstr. 3, 91058, Erlangen, Germany*

[e] *Institute of Chemistry, Saint Petersburg State University, 26 Universitetskii Prospect, Saint Petersburg, Petergof, 198504, Russia*

HIGHLIGHTS

- Laser treatment of copper film ensures nanoparticle formation.
- The electrode material exhibits outstanding electrochemical activity towards OER.
- Easy scalable approach is applicable to any shape and size of the substrate.
- Both laser irradiation and copper species presence provide synergistic effect.

GRAPHICAL ABSTRACT

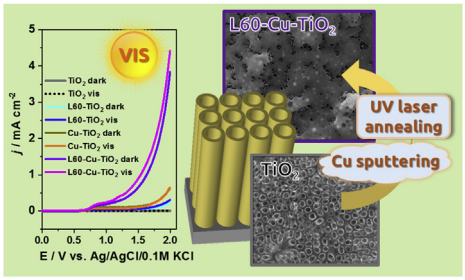

ARTICLE INFO

Article history:
Received 10 April 2020
Received in revised form
1 May 2020
Accepted 6 May 2020
Available online xxx

Keywords:
Laser treatment

ABSTRACT

We proposed fast and scalable route where the ordered TiO_2 nanotubes coated with thin copper layers were annealed by the laser beam of 355 nm wavelength at different fluencies in the range of 15–120 mJ/cm^2. As a result, copper species are integrated with the titania substrate and the formed material exhibits unique optical absorption bands in the visible range. Moreover, X-ray photoelectron spectroscopy analysis reveals the formation of Cu_2O while the 4^+ oxidation state of titanium is preserved. According to the electrochemical results, the material treated by laser exhibits outstanding photoelectrochemical activity comparing to the pristine titania or the one only covered by the thin copper film. In particular, when the fluence of 60 mJ/cm^2 was used for the modification of the titania

* *Corresponding author.*
E-mail address: ksiuzdak@imp.gda.pl (K. Siuzdak).

https://doi.org/10.1016/j.ijhydene.2020.05.054

Please cite this article as: Grochowska K et al., Laser induced formation of copper species over TiO_2 nanotubes towards enhanced water splitting performance, International Journal of Hydrogen Energy, https://doi.org/10.1016/j.ijhydene.2020.05.054

Titania nanotubes
Copper oxide
Water splitting
Visible activity

decorated with Cu film, the current density recorded in KOH electrolyte reaches nearly 4.5 mA/cm^2 at +2.0 V vs. Ag/AgCl/0.1 M KCl upon visible light.

Introduction

Water splitting technology with the assistance of nano-sized materials has a great potential towards the environmentally friendly and low-cost production of hydrogen [1]. This gas is currently regarded as the most promising and green alternative to fossil fuels since the only product of its combustion is water. Moreover, using semiconducting materials that are active under natural light ensures that the generation of charge used further to initiate the splitting process can be supported by solar energy [2]. Since the whole idea of photo-assisted water splitting to hydrogen and oxygen was discovered in 1972 by Honda and Fujishima [3], many approaches have been tested to promote efficient breakage of bonds in water molecule. Among others, titanium dioxide gained wide attention as a promising photoanode due to its high stability, low toxicity and photocorrosion resistance [4]. Moreover, depending on the synthesis protocol, this material can take many geometrical forms: nanoparticles, nanowires, nanobelts or nanotubes [5] offering highly developed surface area. Until now, it has found many applications, for example in solar cells [6], supercapacitors [7], catalysis [8] and water purification [9]. Nevertheless, the main limitation that hampers titania usage in processes supported by light is the absorption within the UV range covering only 5% of the total solar light reaching the Earth. Therefore, various attempts have been undertaken to shift the activity towards longer wavelengths with simultaneous preservation of the material stability.

A number of distinct approaches have been proposed towards this aim: non-metal and metal doping [10], formation of a heterojunction [11] with some other metal oxides or organic materials exhibiting visible light response, e.g. conducting polymers [12] or manipulation with the material morphology leading to a photonic crystal-like behaviour [13]. What is of high importance, if the electrochemical process is foreseen, as in the case of electrochemical water splitting, the material should be also easily deposited onto some conductive substrate. Taking into account facile fabrication method that allows direct formation of the material onto the conductive platform, possible manipulation with the dimensions and wide range of surface modifications the above described requirements are fulfilled by the titania nanotubes (TiO_2NTs) formed during anodization [14–16]. Such an electrochemical synthesis route indeed requires very low-cost equipment and simple electrolyte while the optimized processing parameters, namely voltage, water content or fluorine ion concentration play the most important role. As a result of the anodization, TiO_2 tubes grown directly out of the metal substrate offer their walls and rims surface available for future modification and in consequence tuning of optical, electrical and photoelectrochemical properties is possible. Following that such ordered nanostructures have been utilized in the water splitting process towards both hydrogen [17,18] or oxygen evolution (HER and OER) [19].

According to many literature reports, deposition of metal or metal oxide nanoparticles, electroactive polymers, or doping with metal or non-metal atoms enable formation of completely new material exhibiting much higher visible light absorption, capacitance and/or conductivity comparing to the pristine titania NTs substrate. Recently, decoration of the TiO_2NTs by transition but non-noble metal oxides attracts wide attention. As described in recent reports, deposition of metal oxides such as copper [20,21], iron [22] or nickel [23] oxides can lead to efficient water splitting. Particularly, owing to the incorporation of copper species: Cu [24] as well as CuO [25] nanoparticles, the considerably increased hydrogen generation has been recorded while no deactivation occurs. Thus, since no precious metal is required and the effect is very satisfactory regarding enhanced electrochemical water oxidation, the elaboration of easily scalable methods for TiO_2 modification is of high importance. Taking into account the fact that wet chemistry or electrochemical methods deal with the by-products and electrolyte disposal, respectively, while the modification is performed over the whole sample immersed in the precursor solution, the usage of laser treatment could be regarded as a promising alternative, especially when the modification is conducted directly onto the substrate and within the specified area. Moreover, laser technology is known to be rapid, simple and easily controllable [26] and laser ablation was already successfully used to fabricate OER electrocatalysts [27,28]. However, among different laser-based approaches, pulsed laser induced dewetting (PLiD) technique is very often used towards formation of nanostructures.

PLiD was applied to form metallic nanoparticles for the first time in 1996 by Bischof et al. [29] and further developed by Henley et al. [30,31]. Basically, this process occurs when atomic diffusion takes place. This condition is fulfilled when the liquid layer weakly wets the substrate and at elevated temperatures is thermodynamically unstable and has tendency to form droplets due to the minimization of total interfacial energy of the system. The detailed mechanism of nanoparticle fabrication from a thin metallic layer via the laser approach can be found elsewhere [32]. So far, this technique has been used to obtain e.g. gold, silver, nickel, copper or iron nanoparticles. Nevertheless, the substrates used for metallic film deposition were mostly flat oxides such as SiO_2 or ITO. There are only few reports in which structured substrates (silicon or titanium foil) have been proposed as platforms for PLiD [33,34]. To the best of our knowledge, pulsed

Please cite this article as: Grochowska K et al., Laser induced formation of copper species over TiO_2 nanotubes towards enhanced water splitting performance, International Journal of Hydrogen Energy, https://doi.org/10.1016/j.ijhydene.2020.05.054

laser induced dewetting has not been performed on TiO_2NTs arrays.

Although (as mentioned above) several metals or metal oxides can be used for water splitting, in this work we focused onto copper ones due to the fact that it is cheaper than noble metals, widely used in industry and is Earth-abundant. Moreover, copper and its oxides exhibit a surface plasmon resonance that is observed as a broad absorbance band in the UV–vis range [35]. As a substrate for copper layer magnetron deposition, TiO_2 nanotubes obtained via anodization process were used. UV nanosecond laser was utilized to form nanoparticles and to integrate copper species with TiO_2NTs while Raman spectroscopy was applied to verify the preservation of titania nanotubes anatase phase. The optical properties and energy bandgaps were established from UV–vis spectra. X-ray photoelectron spectroscopy as well as X-ray diffraction techniques were then used to investigate the chemical nature and crystal phase of the material. Finally, electrochemical measurements towards water splitting were conducted both in dark and under visible light irradiation. The obtained results suggest that the prepared electrode material can be successfully used in this kind of application.

Experimental

As a substrate Ti plate (Strem, 99.7%) was used for further growth of titania nanotubes. At first, the metal plates were degreased in acetone, ethanol and deionized water subsequently in each solution placed in ultrasound cleaner for 10 min TiO_2 nanotubes were obtained via single step anodization performed in 2-electrode configuration where Ti plate acts as an anode and rectangular Pt mesh as a cathode. Both electrodes were placed in cylindrical cell filled in electrolyte composed of 0.27 M NH_4F dissolved in the mixture of H_2O/ethylene glycol with the 3:17 v/v volume ratio. The cell was equipped with the thermostatic jacket ensuring the constant temperature of 23 °C during the whole process. After the electrodes immersion in the electrolytic bath, the voltage was increased gradually with 10 mV/s rate up to 40 V and kept constant for 15 min. Afterwards, the voltage was decreased to 0 and the electrodes were taken off the electrolyte. Then, Ti electrode was rinsed in ethanol and air dried. Finally, the as-anodized samples were calcined in the tube electric oven (Nabertherm) at 450 °C for 2 h with the heating rate established to 2°/min.

For further modification, copper 10 nm thin films were deposited using magnetron sputtering machine (Quorum Q150T S) whereas the film thickness was controlled by microquartz balance. Such material labelled as Cu–TiO_2 was used as a substrate for pulsed thermal treatment using Nd:YAG laser ($\lambda = 355$ nm, pulse duration: 6 ns, repetition rate 2 Hz). The process was realized in the vacuum chamber at the pressure of 2×10^{-5} mbar. The samples were placed onto the motorized, computer controlled X/Y table that allows for precise TiO_2NTs plates movement relative to the laser beam. To ensure uniform distribution of laser radiation, the dedicated beam homogenizer was applied within the optical path (laser spot area: 2.4×2.4 mm^2). The table speed was set as 4 mm/min and the overlapping degree between two adjacent laser traces was 10%. The laser treatment of Cu–TiO_2 was realized at different fluences: 15, 30, 60, 120 mJ/cm^2. For reference, the same annealing procedure was realized onto the bare titania without any copper layer.

Measurements

The surface morphology and cross-section were examined using the Schottky field emission scanning electron microscopy (FEI SEM Quanta FEG 250) with an ET secondary electron detector.

The chemical nature of elements and binding properties of the surface were studied using the X-ray photoelectron spectroscopy (XPS), by means of the Escalab 250Xi from ThermoFisher Scientific. High-resolution spectra were recorded at the energy step size of 0.1 eV at a pass energy of 15 eV. The charge compensation was assured through low-energy electron and low-energy Ar^+ ions flow. In order to normalize the spectroscopic measurements, the X axis (binding energy, BE) from XPS spectrum was calibrated for peak characteristics of neutral carbon 1s (BE = 284.6 eV).

The UV–Vis reflectance spectra of titania nanotubes were measured with a dual beam UV–Vis spectrophotometer (Lambda 35, PerkinElmer) equipped with a diffuse reflectance accessory. The spectra were registered in the range of 300–900 nm, with a scanning speed of 120 nm/min. Bandgap energy values were determined as the intercept of the tangent of the plot of transformation of the Kubelka-Munk function. This method was used to determine the bandgap energy for pure and copper modified TiO_2NTs.

The crystal structure of the sample at room temperature was verified by X-ray diffraction (XRD) using Bruker D2 Phaser 2nd generation diffractometer using Cu-Kα radiation and a LynxEye XE-T detector.

The Raman spectra were recorded by a confocal micro-Raman spectrometer (InVia, Renishaw) with sample excitation, by means of an argon ion laser emitting at 514 nm operating at 5% of its total power (50 mW).

Electrochemical measurements were carried out using an AutoLab PGStat 302 N potentiostat-galvanostat system (Methrom, Autolab) in the standard three-electrode assembly, where titanium foil covered by modified nanotubes served as a working electrode (active surface area of 0.4 cm^2). Electrodes were tested in contact with deaerated aqueous 0.5 M Na_2SO_4 and 0.5 M KOH electrolytes. The cyclic voltammetry (CV) curves were registered within the range from −1.0 to +1.0 vs. Ag/AgCl/0.1 M KCl with the scan rate of 50 mV/s while the linear voltammetry (LV) scans were performed using 10 mV/s in the wider potential range from −1.0 toward +2.0 V vs. Ag/AgCl/0.1 M KCl. The LV curves were recorded both in dark and under exposition of working electrode to the visible light generated by the solar simulator (Oriel) equipped with the optical filter eliminating radiation < 420 nm. The photostability test was performed for the most active electrode material under potentiostatic conditions +2.0 V vs. Ag/AgCl/0.1 M KCl.

Moreover, electrochemical impedance spectroscopy (EIS) measurements were performed in the frequency range of 20 kHz–0.1 Hz with 10 mV amplitude at the open circuit

Please cite this article as: Grochowska K et al., Laser induced formation of copper species over TiO_2 nanotubes towards enhanced water splitting performance, International Journal of Hydrogen Energy, https://doi.org/10.1016/j.ijhydene.2020.05.054

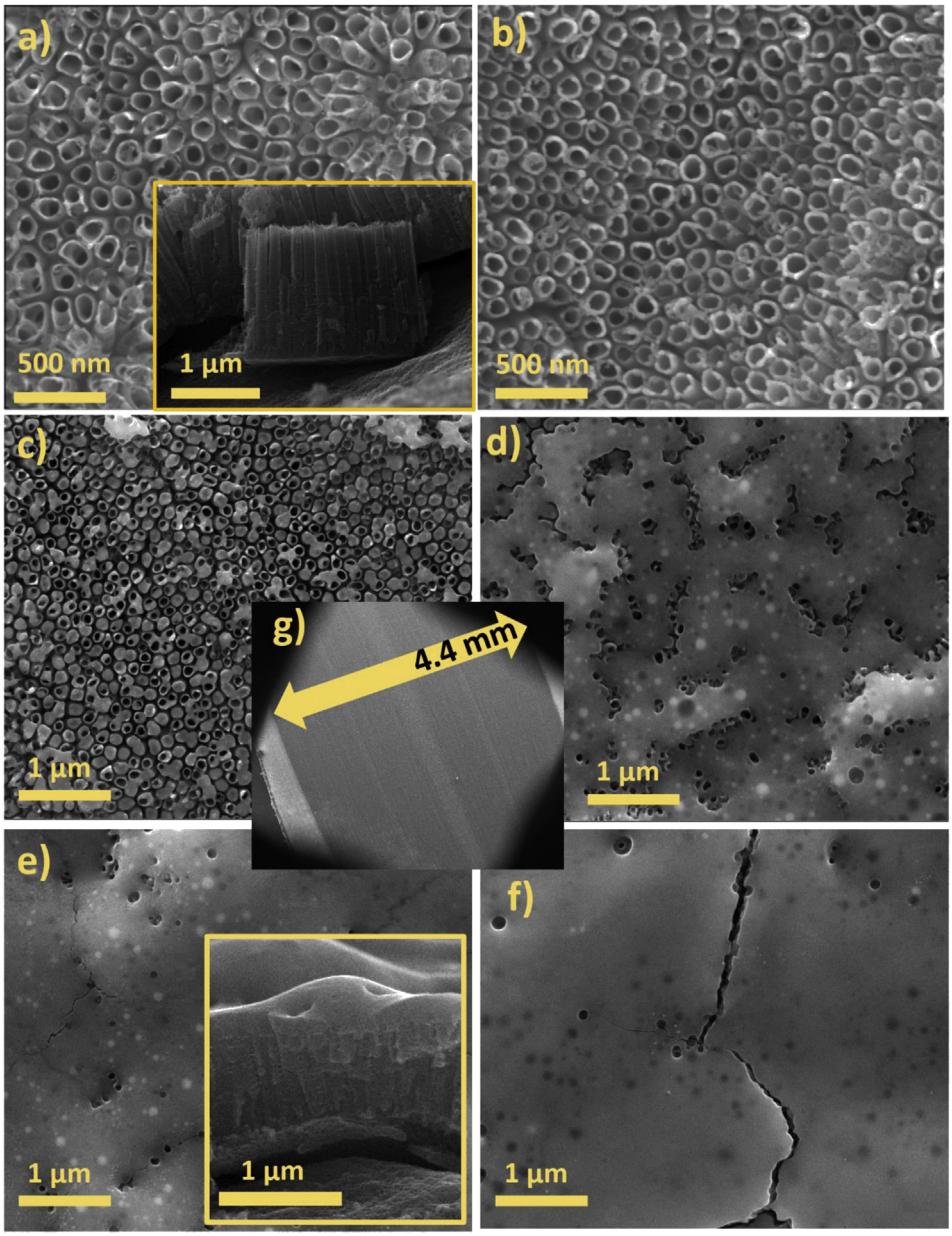

Fig. 1 – SEM images of a) bare TiO_2NTs, b) TiO_2 with evaporated 10 nm thin Cu layer, Cu–TiO_2 treated with laser fluence equalled to c) 15 mJ/cm^2, d) 30 mJ/cm^2, e) 60 mJ/cm^2, f) 120 mJ/cm^2, g) the trance of the laser beam formed onto the TiO_2NTs substrate. Inset: cross-section SEM images of bare untreated and laser treated Cu decorated material at 60 mJ/cm^2.

potential. The EIS spectra were analysed using EIS Analyser [36] with the use of an electric equivalent circuit (EQC). The modified Powell algorithm was used with amplitude weighting r_a:

$$r_a(\omega, P_1 \ldots P_M) = r_c^2 / (N - M) \quad (1)$$

where N is the number of points, M is the number of parameters, ω is the angular frequency, $P_1 \ldots P_M$ are parameters. Parameter r_c is defined as

$$r_c^2 = \sum_{i=1}^{N} \frac{(Z'_i - Z'_{i_{calc}})^2 + (Z''_i - Z''_{i_{calc}})^2}{Z'^2_i + Z'^2_{i_{calc}}} \quad (2)$$

where i corresponds to the measured values of impedance and i_{calc} is attributed to the calculated values; N is the number of points.

Results

Morphology

An optimized one-stage anodization allows one to produce highly uniform layers of aligned TiO_2 nanotubes with the internal diameter of ca. 100 nm and the wall thickness of ca. 18 nm (see Fig. 1 a). The height of unmodified titania tubes reaches ca. 1.5 μm. It can be easily seen in Fig. 1 b that after deposition of 10 nm copper film, the edges of nanotubes

Please cite this article as: Grochowska K et al., Laser induced formation of copper species over TiO_2 nanotubes towards enhanced water splitting performance, International Journal of Hydrogen Energy, https://doi.org/10.1016/j.ijhydene.2020.05.054

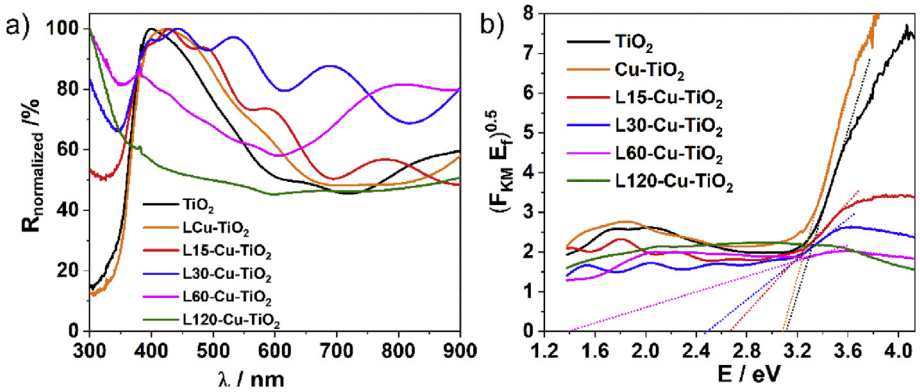

Fig. 2 – a) Reflectance spectra and b) Tauc plots for bare and copper modified TiO_2NTs.

become slightly overgrown while in general the initial architecture of TiO_2NTs remains intact. Application of laser treatment, leads to significant changes in the sample geometry. With the increased fluence of laser irradiation, the melting of the surface becomes more pronounced (see Fig. 1 c-f). Apart from melted layer of TiO_2, one can also observe inhomogeneously distributed spherical or nearly spherical nanoparticles embedded in these layer that can be composed of metal or metal oxide. It should be also noted that for the highest value of laser beam fluence, i.e. 120 mJ/cm^2, some cracks can be seen in the melted film probably due to high temperature stress applied to the material within very short time. Nevertheless, below melted area the ordered structure of TiO_2 is still preserved. From the comparison of cross-section images registered for bare and laser treated samples (Fig. 1 a and e), it can be observed that the length of TiO_2NTs decreases down to ca. 800 nm, that indicates that the surface melted region equals to ca. 200 nm for 60 mJ/cm^2. Moreover, the precisely controlled movement of the sample during laser irradiation enables modification of the material over selected area. Such an approach ensures homogenous treatment within the established surface range. Therefore, for further characterization we limited the irradiation area by two aligned laser traces to ensure the appropriate size of modified sample needed in specific solid state techniques and electrochemical measurements.

Optical properties

In order to study the optical properties of obtained samples, the series of reflectance spectra were recorded and are shown in Fig. 2 a. One may easily notice, that spectrum of pristine titania nanotubes is typical for this kind of material [37]. Large absorption in the UV region can be ascribed to the transition of electron from the valence to the conduction band, while increased absorption from 450 to 900 nm can be related to scattering of light by cracks or pores in the titania arrays [38]. After Cu deposition, the intensity of reflectance spectra slightly decreases in UV region. Moreover, absorption both in UV and vis part of the light spectrum is redshifted. This change can be related to the increased wall thickness of the nanotubes due to Cu layer deposition as mentioned above. Mild laser treatment (15–30 mJ/cm^2) results in appearance of fringes that may be ascribed to formed nanoparticles of Cu or Cu_xO_y (see Fig. 1 c-d). This phenomenon can be explained by: (i) surface plasmon resonance as both metallic and oxide Cu nanoparticles are known to exhibit plasmonic behaviour [39,40] (ii) photonic behaviour of material [41] (i.e. light scattering effect); and (iii) constructive and destructive interference of partially reflected light in the thin films [42]. It should be noted that reflectance of Cu–TiO_2NTs treated with 30 mJ/cm^2 fluence is significantly larger than the one observed for sample modified with 15 mJ/cm^2. With the increase of laser fluence the fringes disappear and the reflectance in UV rises while in the visible light decreases. This could be explained by the presence of remelted layer that can act as a mirror for the selected wavelengths. It can be supported by the fact that titanium dioxide thin films are typically used for such kind of mirrors. Also the surface area of nanotubes covered with remelted layer is smaller than the one of bare NTs. It has been already reported that the reflectance of NTs increases with the decreasing area [43]. Therefore, the increase of absorbance for L60-Cu-TiO_2 and L120-Cu-TiO_2 can be related to the presence of Cu or Cu_xO_y NPs. It can be also observed that the absorption band edges become less sharp with the increased laser fluence that can be attributed to the oxygen deficiency and hence to the presence of Ti^{3+} ions [43].

Basing on the reflectance spectra and using the Kubelka-Munk relation, for all fabricated materials the Tauc plots were prepared and shown in Fig. 2 b. From the analysis of Fig. 2 b, it can be seen that the energy bandgap, E_{bg}, for the pristine TiO_2NTs is narrower than the one reported for bulk anatase (3.2 eV) - see Table 1. This can be related with the electronic structural differences due to the changes in geometry of the material. Moreover, energy bandgap depends also on diameter, wall thickness and length of the NTs as well as the atomic arrangement inside the wall [44]. For almost all laser-modified electrodes, the shift of E_{bg} towards visible region is observed. Only, for L120-Cu-TiO_2 sample it was impossible to estimate this value, as the material absorbs on the same level in the whole wavelength range. Due to the fact the reflectance of prepared material in the UV part of the spectrum is in the range of 50–98%, for further photoelectrochemical tests only vis illumination has been chosen.

Table 1 – The values of bandgap energy determined on the base of Tauc plots (see Fig. 2 b).

Material	E_{bg}/eV
TiO_2	3.11
Cu–TiO_2	3.08
L15-Cu-TiO_2	2.69
L30-Cu-TiO_2	2.48
L60-Cu-TiO_2	1.39
L120-Cu-TiO_2	–

Moreover, although the highest absorption in vis light is exhibited by TiO_2, LCu-TiO_2 and L120-Cu-TiO_2, it is expected that L60-Cu-TiO_2 will have the biggest photoresponse as it exhibits the smallest E_{bg}.

Structural properties

Raman spectra recorded for obtained materials are given in Fig. 3. It can be clearly seen that the presence of Cu layer and further laser treatment do not change the crystal structure and the anatase phase is observable for all prepared samples. Recorded signals at 145, 198, 395, 517 and 635 cm^{-1} are related to the $E_{g(1)}$, $E_{g(2)}$, B_{1g}, A_{1g} and $E_{g(3)}$ active anatase modes, respectively and this is in agreement with previous reports [45–47]. It should be noted that no additional peaks from Cu species arise suggesting that metal or metal oxides do not embed inside titanium dioxide structure. Moreover, mild laser irradiation results in the enhancement of Raman signal and narrowing of linewidth what is consistent with other researchers works. Zhang et al. reported that for TiO_2 nanocrystals the intensity of the lowest frequency Eg mode increases significantly with the increased temperature of annealing [48]. The analogue can be done for laser treated samples, as the rapid temperature growth occurs when the laser interaction with matter takes place. Nevertheless, for higher fluences, i.e. 60 and 120 mJ/cm^2, drastic decrease of signal intensity is observed in comparison with samples treated with 30 mJ/cm^2. This effect may be caused by the changes of the geometry of the titania material as the nanotubes are covered with remelted thin layer with embedded Cu/Cu_xO_y nanoparticles which hampers the overall signal originating from the studied material. Moreover, crystal structure of the sample could be destroyed due to the heat accumulation at the top of the nanotubes. It should be reminded that the laser processing took place in vacuum conditions and therefore the heat exchange with surrounding is limited. Additionally, no shift of Raman frequency and no peaks from rutile are observed for all samples.

In order to confirm the presence of crystalline phase of TiO_2 and Cu/Cu_xO_y species as well as to establish their nature, XRD patterns were recorded and shown in Fig. 4. The detailed labelling of all the arising peaks for the L120-Cu-TiO_2 sample was included as Fig. S1 in ESI file together with the information regarding the JCPDS cards. For pure TiO_2 nanotubes one can ascribe peaks at 25.2°, 38.32°, 48.1° and 54.9° to anatase phase, while at 38.3°, 40.1°, 53.1°, 62.8°, 70.6°, 76.3°, 82.3° and 92.8° to Ti acting here as TiO_2NTs substrate. Moreover, weak peaks at 27.4° and 53.7° correspond to some residual quantities of rutile phase. According to Das et al. [49] the formation of rutile oxide layer is initiated at the Ti/TiO_2NTs interface and therefore some small amount of rutile is not disturbing. The diffraction pattern of pure TiO_2 nanotubes is typical for this kind of material and is consistent with other researchers works [50,51]. After deposition of Cu layer, no additional peaks corresponding to Cu are observed. For laser treated samples (L30-Cu-TiO_2 and L-120-Cu-TiO_2) infinitesimally small peaks at: 29.1° and 35.9° are located and they can be ascribed to cubic fcc structure of Cu_2O, (110) and (111) planes respectively [52]. Nevertheless, it can be assumed that the amount of Cu or Cu_xO_y species is too small to be detected by XRD technique, therefore XPS measurements were conducted.

Characterization of surface chemistry

As has been already announced, high-resolution XPS spectra were recorded in the binding energy range of Ti2*p* (Fig. 5 a), Cu2*p* (Fig. 5 b), O1*s* (Fig. 5 c) and C1*s* (Fig. 5 d) in order to

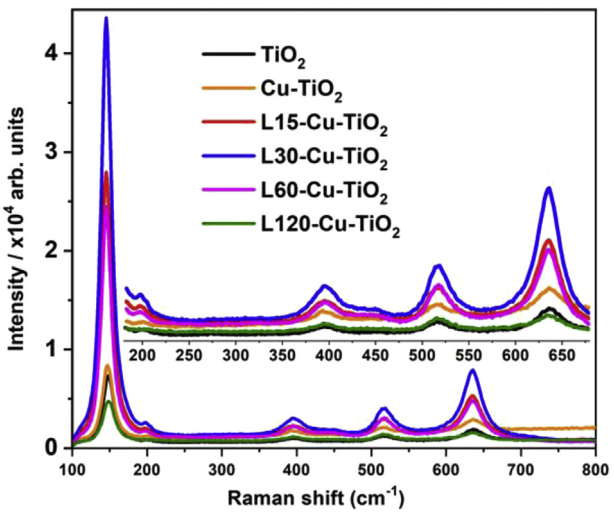

Fig. 3 – Raman spectra of laser treated Cu–TiO_2NTs materials.

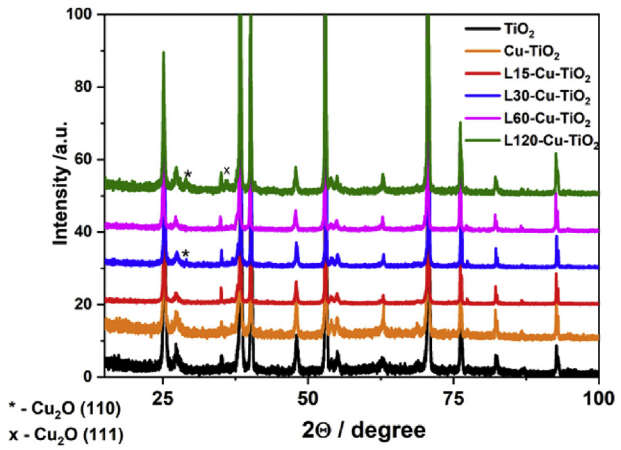

Fig. 4 – XRD pattern recorded for the series of obtained copper modified titania NTs.

Please cite this article as: Grochowska K et al., Laser induced formation of copper species over TiO_2 nanotubes towards enhanced water splitting performance, International Journal of Hydrogen Energy, https://doi.org/10.1016/j.ijhydene.2020.05.054

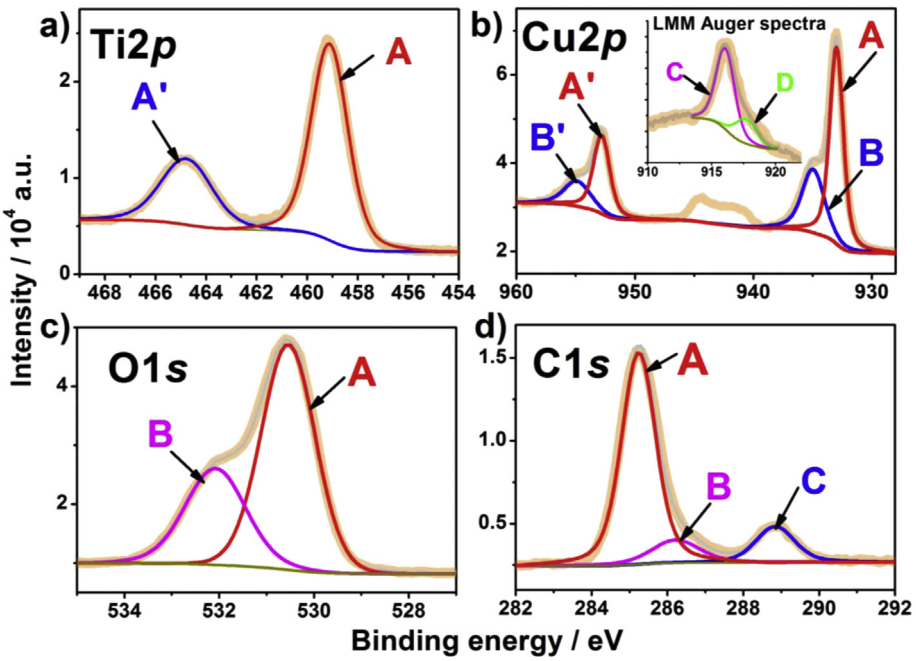

Fig. 5 – XPS including LMM Auger spectra characteristics for Ti2*p*, O1s, C1s and Cu2*p* binding energy region for L60-Cu-TiO_2.

Table 2 – The positions and chemical states of peak maxima for each element found at XPS spectra.

	Ti2*p*3/2	Cu2$p_{3/2}$		O1s	
BE/eV	459.1	933.0	934.9	530.5	532.1
chem. State	TiO_2	Cu_2O	$Cu(OH)_2$	TiO_2/Cu_2O	$Cu(OH)_2$/C–O
at.%	16.6	10.8	5.7	41.3	20.3

determine surface chemistry for L60-Cu-TiO_2 sample selected among others as representative based on both the optical and electrochemical results described later on. The analysis of spectral deconvolution, namely the atomic composition with below described model, is presented in Table 2. The chemistry of titanium reveals a single chemical state of titanium (IV) oxide, while Ti2$p_{3/2}$ peak energy of 459.1 eV is characteristic for stoichiometric titanium dioxide [53–55]. The above results confirm that the structure of TiO_2NTs was not altered by laser-induced formation of copper species on its surface.

Spectral analysis of Cu2*p* BE region reveals the presence of at least two separate chemical states of copper. According to the literature survey the primary component located at 933.0 eV (Cu2$p_{3/2}$ peak acronym A), may correspond to both: metallic copper or copper (I) oxide [56]. For this reason, supplementary analysis was carried out in region characteristic

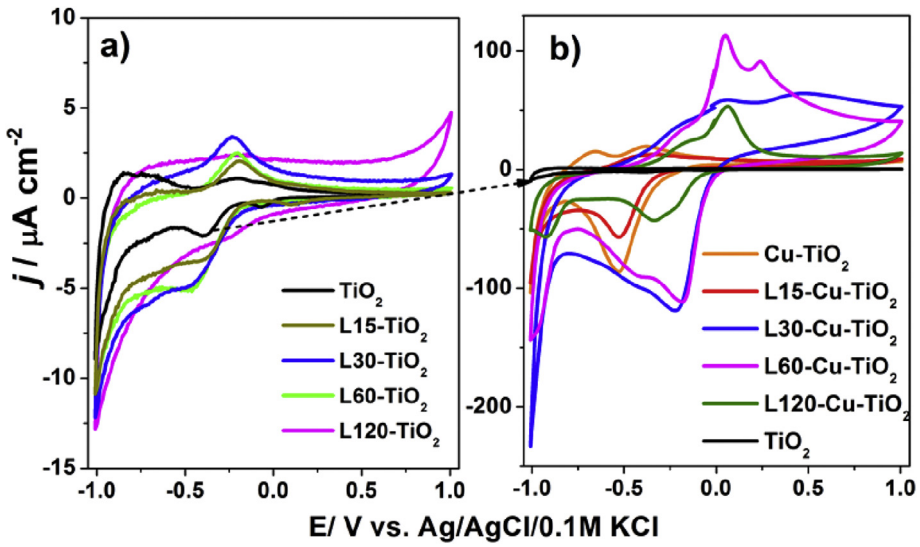

Fig. 6 – Cyclic voltammetry curves registered in 0.5 M K_2SO_4 (50 mV/s) for bare TiO_2NTs and with Cu layer after laser treatment at various fluencies.

Please cite this article as: Grochowska K et al., Laser induced formation of copper species over TiO_2 nanotubes towards enhanced water splitting performance, International Journal of Hydrogen Energy, https://doi.org/10.1016/j.ijhydene.2020.05.054

for the kinetic energy of Cu_{LMM} Auger electrons [57]. The results were plotted in the inset of Fig. 5 b. The two peaks centred at 916.2 (C) and 917.4 eV (D) approach the values of bulk $Cu(OH)_2$ and Cu_2O, respectively [58]. This confirms the primary chemical state of copper present at L60-Cu-TiO_2 surface as Cu_2O. Furthermore, the $Cu2p_{3/2}$ (B) peak shift by +1.6 eV can be recognized as $Cu(OH)_2$, also confirmed by the earlier studies of modified TiO_2 [58]. The paramagnetic Cu^{2+} chemical state is further confirmed by the shake-up satellites located at approx. 944 eV, clearly observed in Fig. 5 b [59]. It should be noted, that the formation of TiO_2–Cu bimetallic nanomosaic should have consequence in the shape and position of $Ti2p_{3/2}$ signal. A binding energy shift towards lower energies (approx. 457.5 eV), which is assisted by increase in observed FWHM. Conversely, the $Cu2p_{3/2}$ A for Cu–TiO_2 is located at approx. 932.5 eV [60,61]. No such shifts were observed in our case, testifying that metal oxides are not embedded inside TiO_2 structure. This is in good agreement to our Raman studies.

Finally, O1s spectrum presented in Fig. 5c confirms previously reported surface chemistry. Two singlet peaks are recognized. The primary component (A) at 530.5 eV is composed of oxygen in TiO_2 lattice [62] and superimposed with the signal originating from Cu_2O [63]. The second peak, located at 532.1 eV corresponds to the oxygen species adsorbed on the surface in the form of non-lattice oxygen, resulting from the nature of the anodization process. The non-lattice oxygen can be found in hydroxyl groups but also partially in some carbon-oxygen species resulting from atmospheric air exposure [64]. The share of adventitious carbon based on C1s peak analysis was not exceeding 15 at.%. The presence of carbon should be considered here as typical contamination for the XPS instrument and due to the anodization nature itself. As was indicated in the experimental section the process was realized in the organic/water electrolyte solution and therefore some carbon residues could remain in the tubular structure [16].

Electrochemical characterization

All the fabricated materials were characterized using cyclic voltamperometry in the wide potential range covering both anodic and cathodic regime (see Fig. 6 a and b). To indicate the influence of the copper species onto the laser treated titania NTs, the electrochemical activity of the reference materials regarded here as the bare TiO_2 nanotubes annealed by 355 nm wavelength with various fluencies is shown in Fig. 6 a. Due to the laser treatment of calcined titania, one may observe the enhancement of peak current density found at the potential of −0.45 V related to the reduction of Ti^{4+} to Ti^{3+} [65]. Moreover, apart from the reduction, the signal attributed to the oxidation is visible. However, when the laser fluence reaches 120 mJ/cm^2, the redox activity is quenched while the electrode keeps capacitive current in the whole potential range.

In the case of main series of samples containing copper, the electrochemical activity of Cu–TiO_2 related with the faradaic reaction is observed only in the cathodic regime of CV. The reduction peak found at −0.52 V vs. Ag/AgCl/0.1 M KCl is associated with two small oxidation humps with maxima registered at −0.66 and at −0.38 V, respectively. Those anodic signals may be ascribed to the formation of Cu(I) when the copper is converted into Cu_2O [66] and it proceeds via two stage process [67]: $Cu + OH^- \rightarrow CuOH + e^-$ and $2CuOH \leftrightarrows Cu_2O + \_H_2O$ while the presence of peak in the reverse scan is due to the reduction of copper (I) to copper (0) forming the bare Cu (111). At positive potentials no other oxidation or reduction activity is observed for Cu–TiO_2 [67]. However, the localization of above listed signals is similar to those recorded in the basic electrolyte where the presence of OH^- ions plays crucial role in the formation of the copper hydroxide and oxide species. Therefore, it may be stated that the hydroxyl groups that cover titania surface can take part in this processes simultaneously affecting the location of oxidation peaks.

The application of the lowest fluence value (15 mJ/cm^2) of laser radiation does not change significantly the character of electrochemical activity and only some enhancement of the reduction peak current density was noticed. When the fluence was increased up to 30 and then to 60 mJ/cm^2, the response of electrode material changes dramatically in terms of both the capacitive current and the location of redox activity. For the sample labelled as L30-Cu-TiO_2, the local maximum at +0.05 V is present while at +0.6 V the highest current density is found within the wide oxidation hump. Regarding the L60-Cu-TiO_2 material, one oxidation peak is present at +0.05 V vs. Ag/AgCl/0.1 M KCl and the other small maximum is located at +0.24 V, whereas at −0.2 V the reduction takes place. According to the Bard et al. [68] and Naseer et al. [69] following equilibriums are expected at copper/electrolyte interface in neutral chloride-free solution:

$$2Cu + H_2O = Cu_2O + 2H^+ + 2e^-$$

$$Cu_2O + H_2O = 2CuO + 2H^+ + 2e^-$$

$$Cu_2O + 3H_2O = 2Cu(OH)_2 + 2H^+ + 2e^-$$

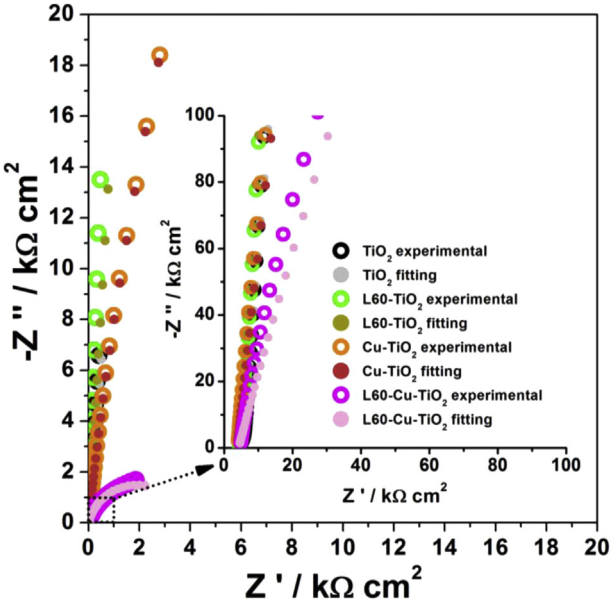

Fig. 7 – a) EIS spectra recorded for the obtained materials in 0.5 M K_2SO_4 accompanied with data obtained from the fitting procedure based on the EQCs (inset).

Table 3 – The values of the selected parameters obtained from the fitting procedure based on the proposed EQC.

sample	Re/ Ω cm^2	CPE/ Ω cm^{-2}s^n	N	R_{ct}/Ω cm^2	C_{eff}/ F cm^{-2}
TiO_2	5.35	2.42×10^{-4}	0.951	8.94×10^{14}	1.71×10^{-4}
L60-TiO_2	4.62	1.19×10^{-4}	0.963	4.92×10^{13}	8.90×10^{-5}
Cu–TiO_2	3.80	8.31×10^{-6}	0.933	3.96×10^{5}	3.95×10^{-6}
L60-Cu-TiO_2	4.22	3.33×10^{-5}	0.844	3.79×10^{4}	6.42×10^{-6}

Therefore, those oxidation peaks found at +0.05 and +0.24 V could be interpreted as following changes in the oxidation state: Cu/Cu^{II} and Cu^{I}/Cu^{II} while the wide oxidation hump arises due to the formation of soluble compound in the redox reaction $Cu + 3OH^- \rightarrow HCuO_2^- + H_2O + 2e^-$. The reduction maximum refers to the Cu(II) towards Cu (I) transformation. Described here activity of copper is typical when the basic electrolyte is used [67] and the hydroxide ions react with copper. Nevertheless, similar activity was found for glassy carbon with incorporated copper species that underwent quasi reversible redox processes [70] in buffered electrolyte at pH 5 or for Cu (111) single crystal in 0.1 M $NaClO_4$ [71]. On the other hand, almost identical shape of cyclic voltammetry was recorded for Cu_2O obtained via electrochemical deposition from the copper sulphate basic solution [72]. According to Wu et al. the peak located at +0.05 V refers to the oxidation of Cu_2O to CuO whereas further wide hump with maximum at +0.6 V vs. Ag/AgCl/0.1 M KCl characteristic for L30-Cu-TiO_2 may be ascribed to the dissolution of CuO to Cu^{2+}: $Cu_2O + H_2O = 2Cu^{2+} + 2e^- + 2OH^-$. Nevertheless, we believe that in the case of Cu–TiO_2 treated with 60 mJ/cm^2 fluence the signals observed at +0.05 and +0.24 V could be recognized rather as two adjacent peaks that were formed via splitting of anodic one referring to Cu(I) to Cu(II) oxidation. Such behaviour is analogous to the one investigated by Wu et al. [72] for Cu_2O film and similar interpretation was proposed in there. On the reverse scan, the reduction is identified with the transformation of CuO to Cu_2O. Additionally, as was observed by Wang et al. for his cuprous oxide electrode material, we also did not notice any current diminution upon consecutive scans proving its electrochemical stability. Comparable redox character of the material containing copper species was also reported by Gentil et al. [73] for Cu based complexes in neutral electrolyte and by Pape et al. [74] in aqueous-organic electrolyte and also interpreted as Cu(II)/Cu(I) couple activity. In the case of the highest laser fluence used for the treatment of Cu–TiO_2 material surface, the current density decreases significantly, but still reversible redox behaviour was observed. Taking into account the outstanding electrochemical activity, the Cu–TiO_2 annealed at 60 mJ/cm^2 was used for further electrochemical studies.

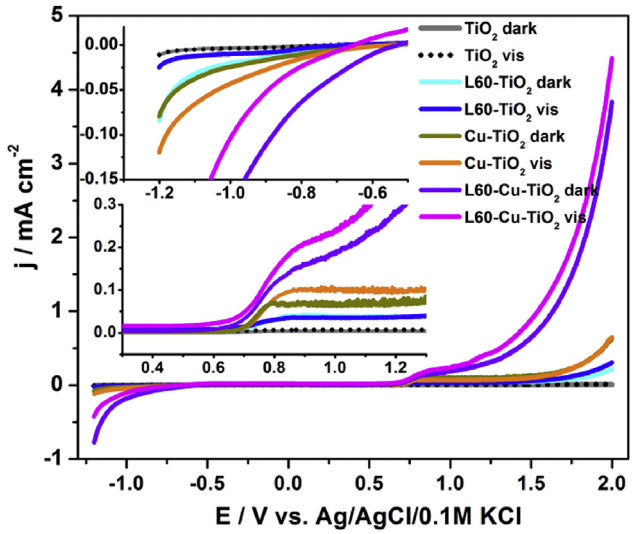

Fig. 8 – Linear voltammetry curves recorded in 0.5 M KOH for selected samples.

In order to gain more information about the electrochemical activity of the laser annealed titania material, the impedance spectra were recorded at open circuit conditions and presented in Fig. 7. The fitting procedure was based on the equivalent electric circuits (EQCs) composed of the following elements: electrolyte resistance (R_e), constant phase element (CPE) and charge transfer resistance (R_{ct}) arranged as given as an inset in Fig. 7. In our modelling we used simplified EQC as has been already applied by Berain et al. [75], Song et al. [76], Ben Taieb et al. [77] and very similar to one provided by Sophia et al. [78] The values of particular elements obtained from the fitting procedure are listed in Table 3. The usage of the electric circuit characterized by one-time constant is possible because of partial overlapping of the time constants representing to the Ti/TiO_2 interface, titania nanotubes and copper species. This statement is supported also by the shape of the impedance spectra in the Nyquist projection. The goodness of fitting (χ^2) is on the level of 10^{-3}–10^{-4} and could be regarded as satisfying to interpret particular elements as real physical process.

The R_e is ascribed to the electrolyte resistance and takes typically low value (3.8–5.35 Ω cm^2) similar for all the investigated electrodes. The CPE element describes here capacitive dispersion which may result from the overlapping time constants due to the high heterogeneity of the surface, as has been already mentioned. The impedance of CPE element is given in the following equation: $Z = Q^{-1}(i\omega)^{-n}$ where the frequency dispersion is expressed in n and ω stays for angular frequency. When n = 1, Q is identified with capacitance, while for the used procedure n is below 1 that reflects both porous nature of the working electrode as well as its heterogeneity. Taking into account the relation provided by Hirshorn et al. [79]:

$$C_{eff} = Q^{1/n}\left(\frac{R_e R_{ct}}{R_e + R_{ct}}\right)^{(1-n)/n}$$

the effective capacitance (C_{eff}) was calculated and also included in Table 3. The highest effective capacitance value is found for bare titania while the lowest one was determined for titania NTs only with the sputtered Cu layer. The highest C_{eff} value found for TiO_2NTs results from the hollow like tubular structure, where the largest developed surface area is

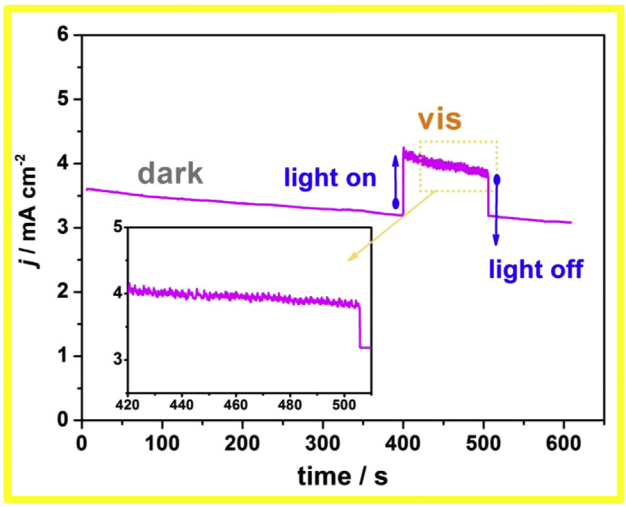

Fig. 9 – The chronoamperometry curve recorded for L60-Cu-TiO_2 at +2.0 V vs. Ag/AgCl/0.1M KCl in dark and under temporary irradiation by visible light.

accessible for the formation of electric double layer. When the copper species are deposited or laser treatment is applied, the titania surface is hidden or even sealed because of the partial melting. This surface partial melting as well as copper species act here as a barrier layer that hamper facile penetration of electroactive species into the free space within tubes. This interpretation is in line with the values of n parameters, where the lowest one is found for the laser treated Cu–TiO_2 material and the highest for unmodified substrate. The last parameter, R_{ct} is assigned to charge transfer resistance and takes value even below 40 kΩ cm^2 for L60-Cu-TiO_2 sample indicating that the transfer of charge proceeds the most easily in this material. It should be underlined that the difference between pristine TiO_2 and the laser and copper modified ones reaches ten orders of magnitude. Such an accelerated charge transfer will affect efficient separation of the e-h pair photogenerated at the electrode/electrolyte interface. Therefore, the higher photoactivity of the L60-Cu-TiO_2 can be expected.

Realizing the outstanding properties of Cu–TiO_2NTs sample modified with 60 mJ/cm^2 fluence, the possible application for electrochemical water splitting was verified in the basic solution. In order to show the sample activity towards the oxygen evolution reaction, LV was performed up to +2.0 V vs. Ag/AgCl/0.1 M KCl (see Fig. 8). The activity of the pristine titania even at high anodic potential is very low and does not exceed 10 μA/cm^2 also in the case when the electrode is exposed to visible light due to its wide bandgap energy. When the titania was treated by laser beam or the 10 nm thin copper film was deposited, the activity towards the electrochemical water splitting is enhanced and at the highest anodic polarization the current density equals 0.22 and 0.62 mA/cm^2, respectively. Nevertheless, visible light affects positively only laser annealed bare TiO_2NTs leading to the activity enhancement to 0.3 mA/cm^2. Regarding the L60-Cu-TiO_2 sample, the dark current density at +2.0 V reaches even 3.83 mA/cm^2 while electrode exposition to light >420 nm improves recorded current density and the value of 4.43 mA/cm^2 is obtained. Typically, electrodes composed of titania nanotubes modified with Cu_2O are characterized towards photoelectrochemical oxidation [20] and hydrogen generation [80]. According to Wang et al. [81] and Zhang et al. [82] the modification by Cu_2O enables current increase induced by the visible light irradiation but in the higher anodic regime the plateau is reached and further polarization does not change the response significantly. It should be also pointed out, that copper oxide apart from most known n-type nature can also behave as a n-type semiconductor [83] substantially affecting the final material photoresponse. Thus, the observed overall photoactivity in the anodic regime could result also from the formation of n-n isotype heterojunction of the well aligned band structure as was identified in the case of Ag_3PO_4/Fe_2O_3 [84] or nSiNWs/TiO_2 [85].

To the best of our knowledge, similar features to our results have not been presented for such heterojunction. In the case of our laser treated material, the superior improvement both in electrochemical and photoelectrochemical activity is observed. The sample L60-Cu-TiO_2 exhibits the enhancement of the current density registered in dark and under irradiation by 6.1 and 7 times, respectively, comparing to the material before annealing. The comparison of this result with the activity of bare TiO_2NTs is crushing and indicates how significantly the electrode performance can be improved.

To verify the stability of the most photoactive laser treated material, the current response was recorded under the L60-Cu-TiO_2 polarization at +2.0 V vs. Ag/AgCl/0.1 M KCl both keeping sample in dark and for some time irradiate it by the light >420 nm. The appropriate chronoamperometry curves is shown in Fig. 9. As can be observed the electrode keeps its current response quite well. When sample was exposed to the visible light irradiation, the enhancement of current density is observed and maintained till the shutter interrupts the access of light to the electrode surface. Basing on this simple experiment, we can regard the material as stable in the OER regime. Therefore, proposed fabrication route enables impressive achievement that can be justified by the unique synergistic effect of changes induced in morphology, structure and optical features upon copper sputtering and further laser treatment with particular parameters.

Conclusions

The preparation and properties of highly reproducible substrates composed of ordered titanium dioxide nanotubes covered with copper species were demonstrated within this work. One-step anodization that lasted only 15 min was utilized to obtain ordered TiO_2NTs while magnetron sputtering and pulsed laser induced dewetting techniques for copper deposition and further sample modification, respectively. SEM inspection revealed formation of remelted TiO_2 layer with nanoparticles that can be composed of metal oxide. XPS and XRD measurements confirmed the presence of Cu_2O. Meanwhile, Raman investigation showed that metal oxide nanoparticles do not embed into TiO_2 structure. From optical properties analysis, the sample exhibiting the lowest energy bandgap value was selected. Moreover, the shift of absorbance band towards visible wave range was observed for laser

modified samples. Sample characterized with the smallest energy bandgap also demonstrated the most pronounced electrochemical activity in terms of increased current density and enhanced (up to 7 times) response in dark conditions and under simulated solar light illumination in comparison to non-modified material. The shape of the recorded cyclic voltammetry scans reveals the formation of stable Cu_2O while impedance studies show reduced resistance and improved space charge capacitance of the copper rich coverage formed over TiO_2NTs support. Obtained results indicate that electrode performance can be significantly enhanced due to the synergistic effect between laser induced morphological changes and optical as well as electrochemical properties affected by the presence of Cu species over the titania support. It should be also emphasized that all processes leading to final material fabrication, i.e. anodization, magnetron deposition, laser treatment, are well known and already employed in industry. The usage of pure copper plate and the magnetron sputtering as well as laser annealing realized in closed space do not led to formation of by-products and negative environmental impact. Furthermore, application of laser enables the intense light treatment over the selected area of desired shape and size by using appropriate masks and moveable system that can open new possibilities in the surface modification of nanomaterials and in consequence in designing of highly active platforms dedicated for water splitting.

Acknowledgements

This work received financial support from the Polish National Science Centre: Grant No. 2017/26/E/ST5/00416.

Appendix ASupplementary data

Supplementary data to this article can be found online at https://doi.org/10.1016/j.ijhydene.2020.05.054.

REFERENCES

[1] Mao SS, Shen S, Guo L. Nanomaterials for renewable hydrogen production, storage and utilization. Prog Nat Sci: Mater Int 2012;22:522–34. https://doi.org/10.1016/j.pnsc.2012.12.003.
[2] Peter LM, Upul Wijayantha KG. Photoelectrochemical water splitting at semiconductor electrodes: fundamental problems and new perspectives. ChemPhysPhysChem 2014;15:1983–95. https://doi.org/10.1002/cphc.201402024.
[3] Fujishima A, Honda K. Electrochemical photolysis of water at a semiconductor electrode. Nature 1972;238:37–8. https://doi.org/10.1038/238037a0.
[4] Ali I, Shuhail M, Altohman ZA, Alwarthan A. Recent advances in syntheses, properties and applications of TiO_2 nanostructures. RSC Adv 2018;8:30125–47. https://doi.org/10.1039/C8RA06517A.
[5] Ge M, Cao C, Huang J, Li S, Chen Z, Zhang KQ, Al-Deyab SS, Lai Y. A review of one-dimensional TiO_2 nanostructured materials for environmental and energy applications. J Mater Chem 2016;4:6772–801. https://doi.org/10.1039/C5TA09323F.
[6] Bai Y, Mora-Sero I, De Angelis F, Bisquers J, Wang P. Titanium dioxide nanomaterials for photovoltaic applications. Chem Rev 2014;114:10095–130. https://doi.org/10.1021/cr400606n.
[7] Clement Raj C, Prasanth R. Review - advent of TiO_2 nanotubes as supercapacitor electrode. J Electrochem Soc 2018;165:E345–58. https://doi.org/10.1149/2.0561809jes.
[8] Nakata K, Fujishima A. TiO_2 photocatalysis: design and applications. J Photochem Photobiol C Photochem Rev 2012;13:169–89. https://doi.org/10.1016/j.jphotochemrev.2012.06.001.
[9] Lee S, Park S. TiO_2 photocatalyst for water treatment applications. J Ind Eng Chem 2013;19:1761–9. https://doi.org/10.1016/j.jiec.2013.07.012.
[10] Basavarajappa PS, Patil SB, Ganganagappa N, Raghava Reddy K, Raghu AV, Ragh AV, Reddy Ch V. Recent progress in metal-doped TiO_2, non-metal doped/codoped TiO_2 and TiO_2 nanostructured hybrids for enhanced photocatalysis. Int J Hydrogen Energy 2019. https://doi.org/10.1016/j.ijhydene.2019.07.241.
[11] Wang CC, Chou CY, Yi SR, Chen HD. Deposition of heterojunction of ZnO on hydrogenated TiO_2 nanotube arrays by atomic layer deposition for enhanced photoelectrochemical water splitting. Int J Hydrogen Energy 2019;44:28685–97. https://doi.org/10.1016/j.ijhydene.2019.09.133.
[12] Shankar K, Mor GK, Prakasam HE, Varghese OV, Grimes CA. Self-assembled hybrid polymer-TiO_2 nanotube array heterojunction solar cell. Langmuir 2007;23:12445–9. https://doi.org/10.1021/la7020403.
[13] Kim WT, Choi WY. Fabrication of TiO_2 photonic crystal by anodic oxidation and their optical sensing properties. Sensor Actuator Phys 2017;260:178–84. https://doi.org/10.1016/j.sna.2017.04.039.
[14] Jun Y, Park JH, Kang MG. The preparation of highly ordered TiO_2 nanotube arrays by an anodization method and their applications. Chem Commun 2012;48:6456–71. https://doi.org/10.1039/C2CC30733B.
[15] Lee K, Kim D, Schmuki P. Highly self-ordered nanochannel TiO_2 structures by anodization in a hot glycerol electrolyte. Chem Commun 2011;47:5789–91. https://doi.org/10.1039/C1CC11160D.
[16] Lee L, Mazare A, Schmuki P. One-dimensional titanium dioxide nanomaterials: nanotubes. Chem Rev 2014;114:9385–454. https://doi.org/10.1021/cr500061m.
[17] Tan Y, Zhang S, Shi R, Wang W, Liang. Visible light active Ce/$Ce_2O/CeO_2/TiO_2$ nanotube arrays for efficient hydrogen production by photoelectrochemical water splitting. Int J Hydrogen Energy 2016;41:5437–44. https://doi.org/10.1016/j.ijhydene.2016.01.154.
[18] Smith YR, Sarma B, Mohanty SK, Misra M. Single-step anodization for synthesis of hierarchical TiO_2 nanotube arrays on foil and wire substrate for enhanced photoelectrochemical water splitting. Int J Hydrogen Energy 2013;38:2062–9. https://doi.org/10.1016/j.ijhydene.2012.11.045.
[19] Li X, Zhang M, Zhang Y, Yu C, Qi W, Cui J, Wang Y, Qin Y, Liu J, Shu X, Chen Y, Xie T, Wu Y. Controlled synthesis of MnO_2@TiO_2 hybrid nanotube arrays with enhanced oxygen evolution reaction performance. Int J Hydrogen Energy 2018;43:14369–78. https://doi.org/10.1016/j.ijhydene.2018.06.027.
[20] Chang KL, Sun Q, Peng YP, Lai SW, Sung M, Huang CY, Kuo HW, Sun J, Lin YC. Cu_2O loaded titanate nanotube arrays for simultaneously photoelectrochemical ibuprofen oxidation and hydrogen generation. Chemosphere 2016;150:605–14. https://doi.org/10.1016/j.chemosphere.2016.02.016.

[21] Zhang S, Peng B, Yang S, Fang Y, Peng F. The influence of the electrodeposition potential on the morphology of Cu_2O/TiO_2 nanotube arrays and their visible-light-driven photocatalytic activity for hydrogen evolution. Int J Hydrogen Energy 2013;38:13866–71. https://doi.org/10.1016/j.ijhydene.2013.08.081.
[22] Hiltunen A, Ruoko TP, Livonen T, Lahtonen K, Ali-Loytty H, Sarlin E, Valden M, Leskela M, Tkachenko N. Design aspects of all atomic layer deposited TiO_2-Fe_2O_3 scaffold-absorber photoanodes for water splitting. Sustain Energy Fuels 2018;2:2124–30. https://doi.org/10.1039/C8SE00252E.
[23] Nail BA, Fields JM, Wang J, Greaney MJ, Brutchey RL, Osterloh FE. Nickel oxide particles catalase photochemical hydrogen evolution from water-nanoscale promotes p-type character and minority carrier extraction. ACS Nano 2015;9:5135–42. https://doi.org/10.1021/acsnano.5b00435.
[24] Zhang S, Peng B, Yang S, Wang H, Yu H, Fang Y, Peng F. Non-noble metal copper nanoparticles-decorated TiO_2 nanotube arrays with plasmon-enhanced photocatalytic hydrogen evolution under visible light. Int J Hydrogen Energy 2015;40:303–10. https://doi.org/10.1016/j.ijhydene.2014.10.122.
[25] Xu S, Jianhong Du A, Liu J, Ng J, Sun DD. Highly efficient CuO incorporated TiO_2 nanotube photocatalyst for hydrogen production from water. Int J Hydrogen Energy 2011;36:6560–8. https://doi.org/10.1016/j.ijhydene.2011.02.103.
[26] Wu J, Yin K, Li M, Wu Z, Xiao S, Wang H, Duan J-A, He J. Under-oil self-driven and directional transport of water on a femtosecond laser-processed superhydrophilic geometry-gradient structure. Nanoscale 2020;12:4077–84. https://doi.org/10.1039/C9NR09902F.
[27] Li Y, Zhou X, Qi W, Xie H, Yin K, Tong Y, He J, Gong S, Li Z. Ultrafast fabrication of Cu oxide micro/nano-structures via laser ablation to promote oxygen evolution reaction. Chem Eng J 2020;383:123086. https://doi.org/10.1016/j.cej.2019.123086.
[28] Wu H, Yin K, Qi W, Zhou X, He J, Li J, Liu Y, He J, Gong S, Li Y. Rapid fabrication of Ni/NiO@CoFe layered double hydroxide hierarchical nanostructures by femtosecond laser ablation and electrodeposition for efficient overall water splitting. ChemSusChem 2019;12:2773–9. https://doi.org/10.1002/cssc.201900479.
[29] Bischof J, Scherer D, Herminghaus S, Leiderer P. Dewetting modes of thin metallic films: nucleation and spinodal dewetting. Phys Rev Lett 1996;77:1536–9. https://doi.org/10.1103/PhysRevLett.77.1536.
[30] Henley SJ, Carey JD, Silva SRP. Pulsed-laser-induced nanoscale island formation in thin metal-on-oxide films. Phys Rev B 2005;72:195408. https://doi.org/10.1103/PhysRevB.72.195408.
[31] Henley SJ, Carey JD, Silva SRP. Metal nanoparticle production by pulsed laser nanostructuring of thin metal films. Appl Surf Sci 2007;253:8080–5. https://doi.org/10.1016/j.apsusc.2007.02.132.
[32] Ruffino F, Carria E, Kimiagar S, Crupi I, Simone F, Grimaldi MG. Formation and evolution of nanoscale metal structures on ITO surface by nanosecond laser irradiations of thin Au and Ag films. Sci Adv Mater 2012;4:708–18. https://doi.org/10.1166/sam.2012.1342.
[33] Giermann AL, Thompson CV. Solid-state dewetting for ordered arrays of crystallographically oriented metal particles. Appl Phys Lett 2005;86:121903. https://doi.org/10.1063/1.1885180.
[34] Grochowska K, Siuzdak K, Macewicz Ł, Skiba F, Szkoda M, Karczewski J, Burczyk Ł, Śliwiński G. Nanostructuring of thin Au films deposited on ordered Ti templates for applications in SERS. Appl Surf Sci 2017;418:472–80. https://doi.org/10.1016/j.apsusc.2016.12.163.
[35] Jiang Q, Ji C, Riley J, Xie F. Boosting the efficiency of photoelectrolysis by the addition of non-noble plasmonic metals: Al & Cu. Nanomaterials 2019;9. https://doi.org/10.3390/nano9010001.
[36] Bondarenko AS, Ragoisha GA. In: Pomerantsev AL, editor. Progress in chemometrics research. New York: Nova Science Publishers; 2005. p. 89–102.
[37] Siuzdak K, Szkoda M, Lisowska-Oleksiak A, Grochowska K, Karczewski J, Ryl J. Thin layer of ordered boron-doped TiO_2 nanotubes fabricated in a novel type of electrolyte and characterized by remarkably improved photoactivity. Appl Surf Sci 2015;357:942–50. https://doi.org/10.1016/j.apsusc.2015.09.130.
[38] Zhang S, Peng B, Yang S, Wang H, Yu H, Fang Y, Peng F. Non-noble metal copper nanoparticles-decorated TiO_2 nanotube arrays with plasmon-enhanced photocatalytic hydrogen evolution under visible light. Int J Hydrogen Energy 2015;40:303–10. https://doi.org/10.1016/j.ijhydene.2014.10.122.
[39] Sekhon JS, Verma SS. Cu, CuO, and Cu_2O nanoparticle plasmons for enhanced scattering in solar cells. In: Renewable energy and the environment, OSA Technical Digest (CD). Optical Society of America; 2011. https://doi.org/10.1364/E2.2011.JWE22. paper JWE22,.
[40] Boltaev GS, Ganeev RA, Krishnendu PS, Zhang K, Guo C. Nonlinear optical characterization of copper oxide nanoellipsoids. Sci Rep 2019;9:11414. https://doi.org/10.1038/s41598-019-47941-8.
[41] Ferreira de Brito J, Tavella F, Genovese C, Ampelli C, Zanoni MVB, Centi G, Perathoner S. Role of CuO in the modification of the photocatalytic water splitting behavior of TiO_2 nanotube thin films. Appl Catal B Environ 2018;224:136–45. https://doi.org/10.1016/j.apcatb.2017.09.071.
[42] Centi G, Passalacqua R, Perathoner S, Su DS. Oxide thin films based on ordered arrays of 1D nanostructure. A possible approach toward bridging material gap in catalysis. Phys Chem Chem Phys 2007;9:4930–8. https://doi.org/10.1039/B703326P.
[43] Ly NT, Nguyen VC, Dao TH, To LHH, Pham DL, Do HM, Vu DL, Le VH. Optical properties of TiO_2 nanotube arrays fabricated by the electrochemical anodization method. Adv Nat Sci Nanosci Nanotechnol 2014;5:015004. https://doi.org/10.1088/2043-6262/5/1/015004.
[44] Hossain FM, Evteev AV, Belova IV, Nowotny J, Murch GE. Electronic and optical properties of anatase TiO_2 nanotubes. Comput Mater Sci 2010;48:854–8. https://doi.org/10.1016/j.commatsci.2010.04.007.
[45] Molenda Z, Grochowska K, Karczewski J, Ryl J, Darowicki K, Rysz J, Cenian A, Siudak K. The influence of the Cu_2O deposition method on the structure, morphology and photoresponse of the ordered TiO_2NTs/Cu_2O heterojunction. Mater Res Express 2019;6:1250b6. https://doi.org/10.1088/2053-1591/ab6195.
[46] Haryński Ł, Grochowska K, Kupracz P, Karczewski J, Coy E, Siuzdak K. The in-depth studies of pulsed UV laser-modified TiO_2 nanotubes: the influence of geometry, crystallinity, and processing parameters. Nanomaterials 2020;10:430. https://doi.org/10.3390/nano10030430.
[47] Ohsaka T. Temperature dependence of the Raman spectrum in anatase TiO_2. J Phys Soc Jpn 1980;48:1661. https://doi.org/10.1143/JPSJ.48.1661.
[48] Zhang WF, He YL, Zhang MS, Yin Z, Chen Q. Raman scattering study on anatase TiO_2 nanocrystals. J Phys Appl Phys 2000;33:912–6. https://doi.org/10.1088/0022-3727/33/8/305.

Please cite this article as: Grochowska K et al., Laser induced formation of copper species over TiO_2 nanotubes towards enhanced water splitting performance, International Journal of Hydrogen Energy, https://doi.org/10.1016/j.ijhydene.2020.05.054

[49] Das S, Zazpe R, Prikryl J, Knotek P, Krbal M, Sopha H, Podzemna V, Macak JM. Influence of annealing temperatures on the properties of low aspect-ratio TiO_2 nanotube layers. Electrochim Acta 2016;213:452–9. https://doi.org/10.1016/j.electacta.2016.07.135.
[50] Suhaimy SHM, Lai CW, Tajuddin HA, Samsudin EM, Johan MR. Impact of TiO_2 nanotubes' morphology on the photocatalytic degradation of simazine pollutant. Materials 2018;11:2066. https://doi.org/10.3390/ma11112066.
[51] Gu D, Wang Y, Li Z, Liu Y, Wang B, Wu H. UV-light aided photoelectrochemical synthesis of Au/TiO_2 NTs for photoelectrocatalytic degradation of HPAM. RSC Adv 2016;6:63711–6. https://doi.org/10.1039/C6RA12031H.
[52] Meghana S, Kabra P, Chakraborty S, Padmavathy N. Understanding the pathway of antibacterial activity of copper oxide nanoparticles. RSC Adv 2015;5:12293–9. https://doi.org/10.1039/C4RA12163E.
[53] Scanlon DO, Dunnill CW, Buckeridge J, Shevlin SA, Logsdail AJ, Woodley SM, Catlow CRA, Powell MJ, Palgrave RG, Parkin IP, Watson GW, Keal TW, Sherwood P, Walsh A, Sokol AS. Band alignment of rutile and anatase TiO_2. Nat Mater 2013;12:798–801. https://doi.org/10.1038/nmat3697.
[54] Li S, Diebold U. Reactivity of TiO_2 rutile and anatase surfaces toward nitroaromatics. J Am Chem Soc 2010;132:64–6. https://doi.org/10.1021/ja907865t.
[55] Jiang Z, Song Y, Lu F, Fei W, Mengqiong Y, Genxiang L, Qian X, Xiang W, Can L. Photocatalytic degradation of Rhodamine B on anatase, rutile, and brookite TiO_2. Chin J Catal 2011;32:983–91. https://doi.org/10.1016/S1872-2067(10)60222-7.
[56] Tian H, Zhang XL, Scott J, Ng C, Amal R. TiO_2-supported copper nanoparticles prepared via ion exchange for photocatalytic hydrogen production. J Mater Chem 2014;2:6432–8. https://doi.org/10.1039/C3TA15254E.
[57] Diaz G, Perez-Hernandez R, Gomez-Cortes A, Benaissa M, Mariscal R, Fierro JLG. CuO-SiO_2 sol-gel catalysts: characterization and catalytic properties for no reduction. J Catal 1999;187:1–14. https://doi.org/10.1006/jcat.1999.2578.
[58] Biesinger MC. Advanced analysis of copper X-ray photoelectron spectra. Surf Interface Anal 2017;49:1325–34. https://doi.org/10.1002/sia.6239.
[59] Jin Z, Liu C, Qi K, Cui X. Photo-reduced Cu/CuO nanoclusters on TiO_2 nanotube arrays as highly efficient and reusable catalyst. Sci Rep 2017;7:39695. https://doi.org/10.1038/srep39695.
[60] Jeon MK, Park JW, Kang M. Hydrogen production from methanol/water decomposition in a liquid photosystem using the anatase and rutile forms of Cu-TiO_2. J Ind Eng Chem 2007;13:84–91.
[61] Wang Y, Duan W, Liu B, Chen X, Yang F, Guo J. The effects of doping copper and mesoporous structure on photocatalytic properties of TiO_2. J Nanomater 2014;178152. https://doi.org/10.1155/2014/178152.
[62] Siuzdak K, Szkoda M, Lisowska-Oleksiak A, Karczewski J, Ryl J. Highly stable organic-inorganic junction composed of hydrogenated titania nanotubes infiltrated by a conducting polymer. RSC Adv 2016;6:33101–10. https://doi.org/10.1039/C6RA01986B.
[63] Barreca D. CVD Cu_2O and CuO nanosystems characterization by XPS. Surf Sci Spectra 2007;14:41–51. https://doi.org/10.1116/11.20080701.
[64] Barr TL, Seal S. Nature of the use of adventitious carbon as a binding energy standard. J Vac Sci Technol 1995;13:1239. https://doi.org/10.1116/1.579868.
[65] Pelouchova H, Janda P, Wber J, Kavan L. Charge transfer reductive doping of single crystal anatase. J Electroanal Chem 2004;566:73–83. https://doi.org/10.1016/j.jelechem.2003.11.013.
[66] Maurice V, Klein LH, Strehblow HH, Marcus P. In situ STM study of the initial stages of anodic oxidation of Cu(111) in the presence of sulfates. J Electrochem Soc 2003;150:B316–24. https://doi.org/10.1149/1.1576225.
[67] Jafarian M, Rashvand Avei M, Danaee I, Gobal F, Mahjani MG. Electrochemical oxidation of saccharose on copper (hydr) oxide-modified electrode in alkaline media. Chin J Catal 2010;31:1351–7. https://doi.org/10.1016/S1872-2067(10)60125-8.
[68] Bard AJ, Parsons R, Jordan J, editors. Standard potentials is aqueous solution, IUPAC. New York and Basel: Marcel Dekker Inc; 1985.
[69] Naseer A, Khan AY. A study of growth and breakdown of passive film on copper surface by electrochemical impedance spectroscopy. Turk J Chem 2009;33:739–50. https://doi.org/10.3906/sag-1204-20.
[70] Shiu KK, Shi K. Preconcentration and electroanalysis of copper species at electrochemically activated glassy carbon electrodes. Electroanalysis 1998;10:959–64. https://doi.org/10.1002/(SICI)1521-4109(199810)10:14%3C959::AID.ELAN959%3E3.0.CO;2-X.
[71] Chun YS, Robinson IK, Gewirth AA. Comparison of aqueous and native oxide formation on Cu(111). J Chem Phys 1999;110:5952–9. https://doi.org/10.1063/1.478495.
[72] Wu L, Tsui L, Swami N, Zangari G. Photoelectrochemical stability of electrodeposited Cu_2O films. J Phys Chem C 2010;114:11551–6. https://doi.org/10.1021/jp103437y.
[73] Gentil S, Molloy JK, Carriere M, Hobballah A, Dutta A, Cosnier S, Shaw WJ, Gellon G, Belle C, Artero V, Thomas F, Le Goff A. Nanotube-supported dicopper complex enhances Pt-free molecular H_2/air fuel cells. Joule 2019;3:2020–9. https://doi.org/10.1016/j.joule.2019.07.001.
[74] Pape VF, Turk D, Szabo P, Weise M, Enyedy EA, Szakacs G. Synthesis and characterization of the anticancer and metal binding properties of novel pyrimidinylhydrazone derivatives. J Inorg Biochem 2015;144:18–30. https://doi.org/10.1016/j.jinorgbio.2014.12.015.
[75] Bervian A, Coser E, Khan S, Pinaro SA, Aguzzoli C. Evolution of TiO_2 nanotubular morphology obtained in ethylene glycol/glycerol mixture and its photoelectrochemical performance. Mater Res 2017;20:962–72. https://doi.org/10.1590/1980-5373-MR-2016-0878.
[76] Song J, Zheng M, Yuan X, Li Q, Wang F, Ma L, You Y, Liu S, Liu P, Jiang D, Ma L, Shen W. Electrochemically induced Ti3+ self-doping of TiO2 nanotube arrays for improved photoelectrochemical water splitting. J Mater Sci 2017;52:6976–86. https://doi.org/10.1007/s10853-017-0930-z.
[77] Taieb SB, Assaker IB, Bardaoi A, Gannouni M, Souissi A, Nowak S, Mouton L, ammar S, Chtourou R. Correlation between titanium foil substrate purity and TiO2Nts physical and electrochemical properties for enhanced photoelectrochemical applications. Int J Hydrogen Energy 2016;41:6230–9. https://doi.org/10.1016/j.ijhydene.2016.03.043.
[78] Sophia H, Salian GD, Zazpe R, Prikryl J, Htomadko L, Djenizian T, Macak JM. Macak ALD Al_2O_3-coated TiO_2 nanotube layers as anodes for lithium-ion batteries. ACS Omega 2017;2:2749–56. https://doi.org/10.1021/acsomega.7b00463.
[79] Hirschorn B, Orazem ME, Tribollet B, Viever V, Frateur I, Musiani M. Determination of effective capacitance and film thickness from constant-phase-element parameters. Electrochim Acta 2010;55:6218–27. https://doi.org/10.1016/j.electacta.2009.10.065.
[80] Dubey PK, Kumar R, Tiwari RS, Strivastava ON, Pandey AC, Singh P. Surface modification of aligned TiO_2 nanotubes by Cu_2O nanoparticles and their enhanced photo

Please cite this article as: Grochowska K et al., Laser induced formation of copper species over TiO_2 nanotubes towards enhanced water splitting performance, International Journal of Hydrogen Energy, https://doi.org/10.1016/j.ijhydene.2020.05.054

electrochemical properties and hydrogen application. Int J Hydrogen Energy 2018;43:6867–78. https://doi.org/10.1016/j.ijhydene.2018.02.127.

[81] Wang M, Sun L, Lin Z, Cai J, Xie K, Lin C. p-n heterojunction photoelectrode composed of Cu_2O-loaded TiO_2 nanotubes arrays with enhanced photoelectrochemical and photoelectrocatalytic activities. Energy Environ Sci 2013;6:1211–20. https://doi.org/10.1039/C3EE24162A.

[82] Zhang J, Wang Y, Yu C, Sh X, Jiang L, Cui J, Chen Z, Xie T, Wu Y. Enhanced visible-light photoelectrochemical behaviour of heterojunction composite with Cu_2O nanoparticles-decorated TiO_2 nanotube arrays. New J Chem 2014;38:4975–84. https://doi.org/10.1039/C4NJ00787E.

[83] McShane CM, Choi KS. Photocurrent enhancement of n-type Cu_2O electrodes achieved by controlling dendritic branching growth. J Am Chem Soc 2009;131:2561. https://doi.org/10.1021/ja806370s.

[84] Yan Y, Guan H, Liu S, Jiang R. Ag_3PO_4/Fe_2O_3 composite photocatalysts with an n–n heterojunction semiconductor structure under visible-light irradiation. Ceram Int 2014;40:9085–100. https://doi.org/10.1016/j.ceramint.2014.01.123.

[85] Yenchalwar SG, Azhagan VK, Shelke MV. Enhanced photoluminescence and photoactivity of plasmon sensitized nSiNWs/TiO_2 heterostructures. Phys Chem Chem Phys 2014;16:17786–91. https://doi.org/10.1039/C4CP01497A.

Please cite this article as: Grochowska K et al., Laser induced formation of copper species over TiO_2 nanotubes towards enhanced water splitting performance, International Journal of Hydrogen Energy, https://doi.org/10.1016/j.ijhydene.2020.05.054